Rheol Acta (2002) 41: 265–275

ORIGINAL CONTRIBUTION

Byung D. Chin
H. Henning Winter

Field-induced gelation, yield stress, and fragility of an electro-rheological suspension

Received: 1 May 2001
Accepted: 11 August 2001

B. D. Chin · H. H. Winter (✉)
Department of Chemical Engineering
University of Massachusetts, Amherst
MA 01003, USA
e-mail: winter@ecs.umass.edu

Abstract Electro-rheological suspensions (ERS) are known to undergo liquid-to-solid transition under the application of an electric field. Long-range interaction between neighboring particles results in sample-spanning particulate structures which behave as soft solids. Here, we studied the rheological expression of this field-induced transition which has many similarities with chemical gelation. This similarity shows in mechanical spectroscopy on a suspension of monodisperse silica in PDMS as model ERS. Upon application of the electric field, dynamic moduli G', G'' grow by orders of magnitude and evolve in a pattern which is otherwise typical for gelation of network polymers (random chemical or physical gelation). At the gel point, the slow dynamics is governed by power-law relaxation behavior (frequency-independent tan δ). A low field strength is sufficient to reach the gel point and, correspondingly, the percolating particle structure at the gel point is still very fragile. It can be broken by the imposition of low stress. For inducing a finite yield stress, the field strength needs to be increased further until the long-range electrostatic interaction generates string-like particle alignments which become clearly visible under the optical microscope. The onset of fragile connectivity was defined experimentally by the tan δ method. The ERS was probed dynamically at low frequencies where the transition is most pronounced, and also in steady shear where the rate of structure formation equals the rate of internal breaking.

Key words Electrorheology · Gelation · Yield stress · Monodisperse particles · Fragility · Suspension

Introduction

Rheology is a most sensitive tool to study the onset of structure formation which eventually results in sample spanning connectivity at the gel point. Most commonly, this transition has been studied with isotropic network materials. However, if the structure is anisotropic, the connectivity develops preferably in one direction while perpendicular connectivity remains low. Such anisotropic solidification process has been established in electro-rheological suspensions (ERS) of semiconducting or dielectric particles in a non-conducting fluid (Winslow 1949; Block and Kelly 1988). When mounting an ERS between two parallel electrodes, an electric field can induce string-like particulate structures parallel to the field lines. The connectivity between the particles in the strings arises from their field-induced dipoles. The particle interaction greatly affects the rheology of the ERS, resulting in an increase of the shear viscosity and, if the developing structure is strong enough, in a liquid-to-solid transition. Linear viscoelastic material functions such as storage modulus, loss modulus, and phase angle

depend on electric field strength, solid concentration, strain amplitude, frequency, and direction of probing.

Pan and McKinley (1997) viewed ERS as anisotropic particulate networks and compared the viscoelasticity of model ERS with that of particle gels, showing the very small critical strain to failure. Pan's proposed model network consists of a primary structure spanning between the electrodes in the direction of the field and a secondary structure of short strings of particles tilted with the field direction (due to many-body effects). Two key factors were found to determine the suspension structure: the attractive force between the particles and the strain level at which the rigidity of the particle structure can persist. Linear viscoelasticity maintained by the preserved structure is restricted to very low strain levels ($\gamma_e = 4 \times 10^{-4}$ to 0.03, Parthasarathy and Klingenberg 1996; $\gamma_e = 0.003$–0.008, Pan and McKinley 1997).

Field-induced forces between particles depend on the dipole moments and the particle distance. Under the point-dipole approximation, the total electrostatic force F_i^e acting on a sphere i is given by $F_i^e = \sum_{j \neq i} F_{ij}^e$ where the electrostatic interaction force (F_{ij}^e) between two adjacent particles (particle i and j, diameter a) is (Klingenberg and Zukoski 1990)

$$F_{ij}^e = 12\pi\varepsilon_0\varepsilon_s\beta^2 a^2 E^2 \left(\frac{a}{r_{ij}}\right)^4 \left[\left(3\cos^2\theta_{ij} - 1\right)e_r^{ij} + \sin 2\theta_{ij} e_\theta^{ij}\right] \tag{1}$$

where ε_0 is the permittivity of free space (8.85×10^{-12} C^2 J^{-1} m^{-1}), r_{ij} is the center-of-mass separation between two particles, θ_{ij} is the angle between the line of centers and the applied electric field E, and e_r^{ij}, e_θ^{ij} are the unit vectors along the axis of r and θ, respectively. Obviously $r_j - r_i = r_{ij} e_r^{ij}$. The relative polarizability β is defined as $(\varepsilon_p - \varepsilon_c)/(\varepsilon_p + 2\varepsilon_c)$, where subscripts p,c denote the particle and continuous phase. The predicted value of stress from the electrostatic force model, Eq. (1), is significantly smaller than experimental values. This might be due to a multipole effect (Klingenberg 1993) which significantly increases the electrical force between particle pairs aligned with the field. Due to the short-range force between neighboring chains, string-like structures attract one another and merge eventually into thick, closely packed columns rather than maintaining a dispersed set of strings (Halsey 1992). The coarsening of individual strings is very pronounced and can be observed in the optical microscope, especially at increased field strength. Not considered in Eq. (1) is the phenomenon that the finite electrical conductivity of ERSs allows charges to migrate across adjacent particles. This effectively screens out some of the dipoles within the particles. The concept of complex permittivity has been introduced for such semi-conducting particles (Davis 1992).

The polarization force in Eq. (1) is decaying as r^{-4}, which is evidently a long-range interaction (Halsey 1992), unlike the short-range interactions between the particles in colloidal dispersions or particulate gel networks. In dipolar fluids such as ERS, an additional short-range interaction exists which drives particles to self-assemble in their thermally fluctuating structures (Tlusty and Safran 2000). However, this is small compared to the long-range interaction (Eq. 1) and corresponding short-range force between parallel strings.

McLeish et al. (1991) proposed the ERS viscoelasticity model as fully aligned single-sphere strings. The storage modulus was determined by electrostatic tension along the string, and was predicted as

$$G' = 3\phi\, e_0 e_c \beta^2 E^\Delta \quad \text{with } \Delta = 2 \tag{2}$$

Electrostatic contributions on the loss moduli G'' were thought to arise from a small fraction of free strings, mostly connected to only one of the electrodes. At low frequency, G'' of the string model depends upon the fraction of free strings and varies proportionally with ω. With the assumption of fluid-dynamic screening, G'' was predicted to depend on ω^0 for a wide range of intermediate frequencies.

Many experiments on ERSs have been explained with the existence of a yield stress (Marshall et al. 1989; Klingenberg and Zukoski 1990; Bonnecaze and Brady 1992; Zukoski 1993). Below a critical yield strain or stress, the ERS can be described as viscoelastic solid. However, the yield values are very low because of the fragility of field-induced internal structure. When broken above the yield stress, the ERS flows (Deinega and Vinogradov 1984; Gamota and Filisko 1991; McLeish et al. 1991). At steady state shearing, ERSs have been simply characterized by a Bingham fluid model (Marshall et al. 1989; Goodwin et al. 1997):

$$\begin{aligned} &\tau = \tau_y + \eta_{pl}\dot{\gamma} \quad \left(\text{for } \tau > \tau_y\right), \text{ and} \\ &\dot{\gamma} = 0 \quad \left(\text{for } \tau < \tau_y\right) \end{aligned} \tag{3}$$

where τ_y is the Bingham yield stress, η_{pl} is the plastic viscosity, $\dot{\gamma}$ is the shear rate, and τ is the shear stress. The exact value of the yield stress has been the subject of dispute; large variations in τ_y were found when choosing different ranges of shear rate. One expects the yield stress τ_y to scale as E^Δ, where $\Delta = 2$ is commonly observed in a low field strength and $1 < \Delta < 2$ in a high field. The plastic viscosity of ERS has been reported to be insensitive to variations in electric field strength and it was found to be approximately identical to the off-field high-shear rate viscosity of the suspension (Parthasarathy and Klingenberg 1996). However, under continuous shear probing, complicated structural processes such as string-rupture and continuous reformation (Bonnecaze and Brady 1992) cause shear-thinning in a wide range of

shear rate. The Herschel-Bulkley shear model can better express this phenomenon, using parameter m and power-law index n (Lee and Wereley 2000):

$$\tau = \tau_y + m|\dot{\gamma}|^{n-1}\dot{\gamma} \quad (4)$$

For steady shear behavior of magneto-rheological (MR) fluids at high magnetic flux, the Herschel-Bulkley model was also fitted successfully (Wang and Gordaninejad 2000).

Unlike most of the ERSs, no yield stress was observed in electro-rheological liquid crystalline polymers. The anisotropy of oriented mesogens parallel to the field direction enhanced the viscosity rather than introducing a finite yield stress (Tse and Shine 2000). An alternative model by Halsey et al. (1992) is based on the formation of condensed drops (prolated ellipsoid) with aggregating dipolar particles. A shear flow tends to rotate the droplets, whereas electric field exerts a restoring torque towards aligned positions along the field direction. The resultant shear-thinning viscosity scaled as power law in shear rate, in agreement with the experimental data. No yield stress was observed for this electro-rheological colloid. This was attributed to the lack of ability for particles to bind to the of electrode surface (Halsey 1992).

There have been few experimental studies on the early stages of field-induced structure formation of ERS due to difficulties in the rheological probing. In this paper, we focused on these early stages, studied the viscoelasticity and structural transition of ERSs in the framework of liquid-to-solid transitions, and compared it with behavior of classical networks of random three-dimensional connectivity. The gel point of a random network distinguishes itself by the divergence of the longest relaxation time and by a power law relaxation time spectrum at long times (Winter and Mours 1997). For connectivity development beyond the classical gel point, solid behavior manifests itself by the appearance and growth of an equilibrium modulus, G_e. The limiting modulus at low frequency, obtained in this study, is conceptually close to the equilibrium modulus. The equilibrium modulus itself could not be obtained due to limitations in the experimentally accessible frequency range as well as in the lack of time-temperature superposition of ERS data. This is the major limitation in the current study.

The gel point can be detected by its power law relaxation behavior in a mechanical spectroscopy experiment. The loss tangent at the gel point is independent of frequency in the terminal relaxation regime and directly related to the relaxation exponent (n_c) (Chambon and Winter 1987):

$$\tan\delta(\omega) = \tan\left(\frac{n_c\pi}{2}\right) \quad (5)$$

for $0 < \omega < 1/\lambda_0$. Similar relaxation patterns are expected for directional gelation of ERSs; however, very little is known about the role of anisotropy.

We focus primarily on the weakly connected internal structure at low field strength near the gel point, its manifestation in dynamic rheology, and the beginning of a yield stress where the material structure can still be easily broken (fragility). These phenomena are best seen in ERS with low particle concentration and at low field strength. Rheological studies are augmented by structural studies under the optical microscope.

Experimental

Electrorheological suspensions (ERS)

Monodisperse, spherical silica particles (Seahostar KP-100 from Nippon Shokubai – amorphous silica with average particle size 1.00 ± 0.10 μm) served as model particles with dielectric polarizability. Silica content is more than 99.9% as SiO_2 (calcinated at 1000 °C according to manufacturer's data). Scanning electron microscopy of the silica particles (Fig. 1) shows the narrow size distribution. The particles were dispersed uniformly in a non-conducting liquid, which is un-crosslinked PDMS, vinyldimethyl-terminated polydimethylsiloxane (United Chemical) with Newtonian viscosity $\eta = 0.5$ Pa.s, by magnetically stirring for about 72 h. Dielectric constant of pure SiO_2 at room temperature is 3.9∼4.0, which is higher than the 2.5∼2.6 of PDMS (Randall et al. 1994). Moreover, absorbed water (8 wt%) on our silica particle surface significantly increased its dielectric constant and conductivity (Ostubo 1992) so that a field can induce ionic polarization. The ERS suspensions contain 10, 20, and 30 wt% of silica particles. Since the density of silica particle and PDMS are 2.0 and 0.96 g/cm^3 (manufacturer's data), the particle volume fractions (ϕ) of the samples corresponds to 0.051, 0.107, and 0.171, respectively. Accordingly, these samples are named ERS051, ERS107, and ERS171.

Experimental apparatus for rheometry

Oscillatory shear was performed in a rotational rheometer (ARES, Rheometric Scientific Inc.) with rigid insulating spacers at the foot of both fixtures where they connect to the transducer or motor (see Fig. 2a). A Couette cell was used for low-viscosity suspensions (ERS051, ERS107); diameters of the cup and bob were 27.0 mm and 25.0 mm, respectively (i.e., the gap size was 1.0 mm). The height of the bob was 32.0 mm. The inner wall of the cup was the

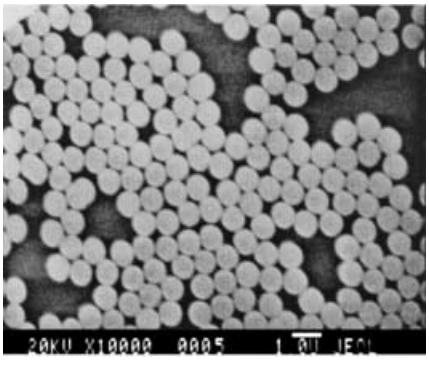

Fig. 1 Scanning electron microscopy of monodisperse silica particles (KP-100)

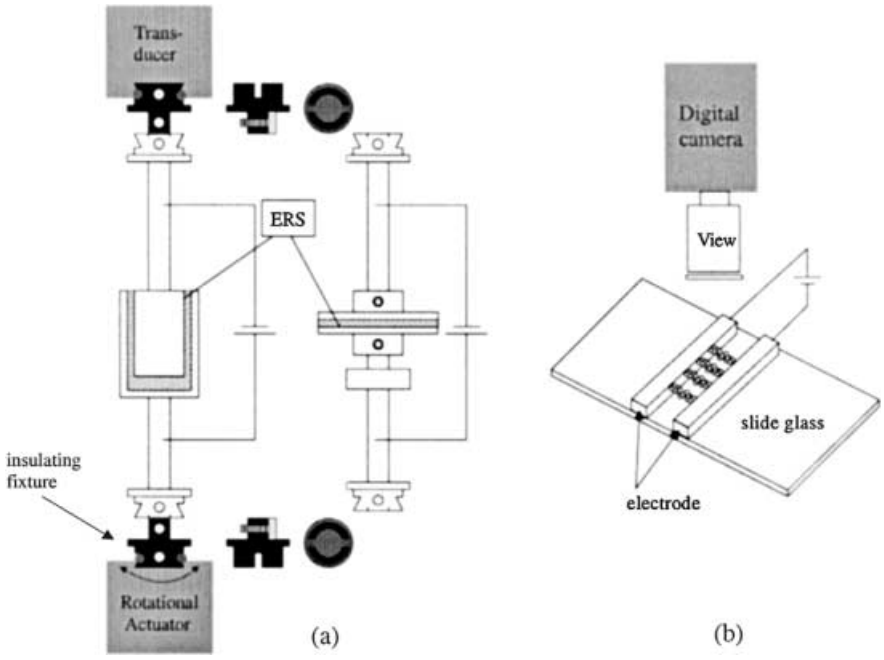

Fig. 2a, b Schematic diagram of the experimental apparatus: **a** modified ARES with Couette geometry and parallel plate fixture; **b** static view cell for microscopic observation

positive electrode and the bob was grounded. For suspensions with volume fraction of $\phi = 0.171$ (ERS171), a parallel plate fixture with 50.0 mm diameter was chosen. A high voltage power supply (Model 215, Bertan) provided the electric field. The magnitude of electric field strength was varied from 30 to 2000 V/mm. For the entire range of volume fraction, the current passing through the sample was below the limit of detection, even at highest field. All of the experiments were performed at room temperature.

Microscopic observation

The formation of particle strings and columns in the electric field and stationary condition was observed with an optical microscope (Carl Zeiss Inc., model ZPU01) equipped with a CCD video camera (Panasonic Inc., WV-BP310). ERS107 was placed between stationary metal electrodes attached to a sheet of glass. The gap between the two electrodes was set to 1.0 mm (see Fig. 2b). Images at increasing field strength were taken of the sample near the center of the gap between two planar electrodes to concentrate on bulk effects (instead of boundary effects). In principle, the inevitable surface roughness of the metal electrode can initiate heterogeneous nucleation of particle strings or even the formation of vortex flow when a strong electric field is applied. However, no such instability was observed with our system.

Rheological measurements (dynamic and steady shear)

The samples were subjected to small amplitude oscillation. The resulting stress was decomposed into an in-phase and out-of-phase contribution, the storage and loss moduli, $G'(\omega)$ and $G''(\omega)$. Small strain amplitude was chosen in order to stay within the linear viscoelasticity range of the ERS. Due to the low torque signal in the low electric field, frequency sweeps ranged from 1.0 to 100 rad/s for $E \leq 250$ V/mm and from 0.1 to 100 rad/s for $E \geq 500$ V/mm. Before each frequency sweep, samples were sheared once at a large amplitude strain ($\gamma = 1$) at 10 rad/s for 60 s. As a result of such initial conditioning, data were highly reproducible. For steady shear experiments, samples were subjected to shear rates from 0.1 to 100 s^{-1} at each field strength.

Results

Linear viscoelastic behavior at small strain

In preparation of the main rheological experiments, the linear viscoelastic range was checked in oscillatory shear at a fixed frequency of 10 rad/s and at increasing strain amplitude (Fig. 3a,b). The electric field strength was varied. Without electric field the dynamic moduli were constant up to a strain amplitude of $\gamma_e = 20\%$. At increasing electric field strength the limiting strain amplitude for the linear viscoelastic range decreased. The field-induced gelation studies below have been performed at low enough strain to ensure linear viscoelastic behavior.

We studied the dynamic moduli during field-induced gelation of three ERS samples. The dynamic moduli grew by orders of magnitude when the electric field strength was increased (Figs. 4, 5, and 6). Without electric field, the suspensions were fluids of very low elasticity. The loss modulus showed the typical power law behavior with $G'' \sim \omega$. The storage modulus was very low and approached $G' \sim \omega^2$ behavior in the terminal zone. The deviation from the ideal ω^2 behavior is attributed to a weak water-bridging effect between the silica particles and the presence of van der Waals interaction, but also shows the limit of sensitivity of the rheometer. The rheometer torque at very low frequency was below the lower limit of the torque transducer and low frequency data are not reported here, especially at low field condition. Increased electric field strength raised the connectivity of the particulate structure and,

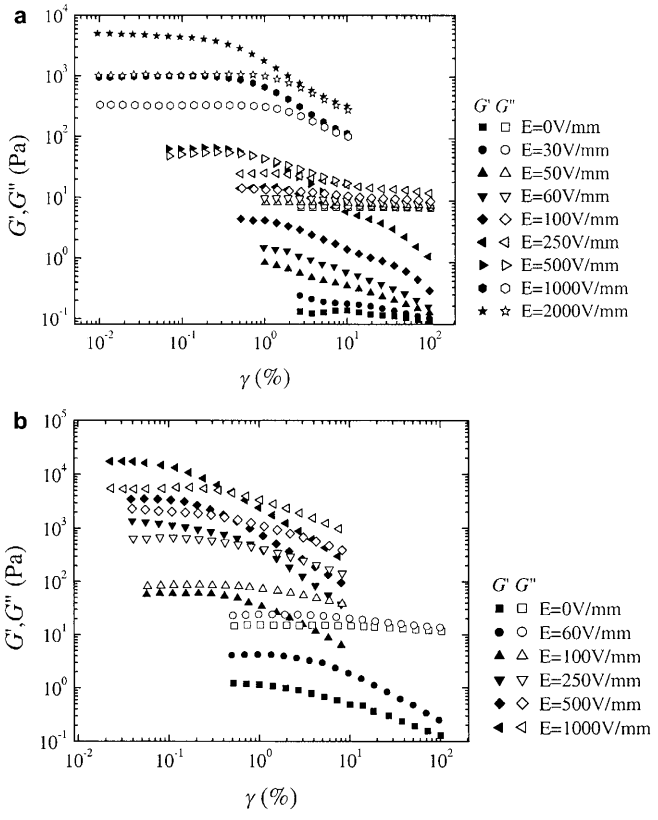

Fig. 3a, b Strain dependence of G', G'' at $\omega = 10$ rad/s: **a** for silica suspension ERS107. A constant modulus value denotes the region linear viscoelasticity, which is limited to about ~10% for $E = 0 \sim 60$ V/mm, $0.1 \sim 1\%$ for intermediate field ($E = 100 \sim 500$ V/mm), and less than 0.5% for $1000 \sim 2000$ V/mm; **b** for ERS171 similar behavior is seen. However, in this relatively concentrated ERS, the linear limit of strain became smaller with electric field strength

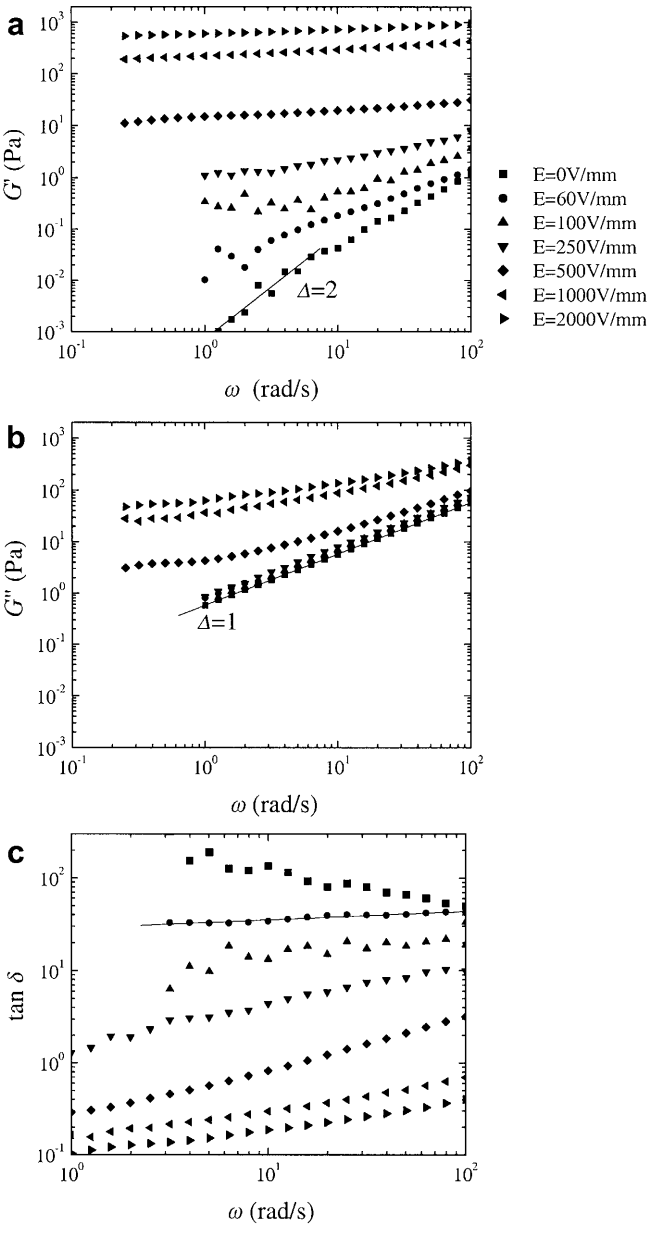

Fig. 4a–c Frequency dependence of linear viscoelastic properties for ERS051 (silica suspension with $\phi = 0.051$): **a** storage moduli G'; **b** loss moduli G''; **c** tan δ. The strain amplitudes vary with field strength, 10% for $E \leq 60$ V/mm, 2% for $E = 100$ and 250 V/mm, 0.8% for $E = 500$ V/mm, 0.4% for $E = 1000$ V/mm, and 0.1% for $E = 2000$ V/mm

hence, G' and G'' grew in magnitude and the terminal (flow) region shifted to lower frequencies.

The evolution of G' and G'' showed the typical features of a liquid-to-solid transition (Fig. 4a,b). At a zero or low electric field, G'' was significantly higher than G' in the entire experimental region. G' began to dominate at higher electric fields. G'' also increased with field strength but much less than G'. The slope of the loss tangent (Fig. 4c) was negative at first, became flat at about $E = 60$ V/mm, and turned positive at higher field strength. At the condition of fully aligned particle strings ($E \geq 1.0$ kV/mm), the slope of G' became close to zero but still it remained a weak function of ω. For ERS107 (Fig. 5a,b,c), the overall tendency was similar but G' and G'' increased more rapidly in the transition region of intermediate electric field strength. The flat tan δ appeared already at a field strength of about $E = 30$ V/mm. Figure 6a,b,c shows the corresponding result of frequency-sweep tests for ERS171. The dynamic moduli were relatively high from the beginning, even without applying the field. With the field, the moduli grew even further. At this volume fraction, the accessible frequencies were not low enough for G' to show the expected ω^2 behavior at zero field strength. Also, the loss tangent (Fig. 6c) did not show any distinct transition in the experimentally accessible frequency range.

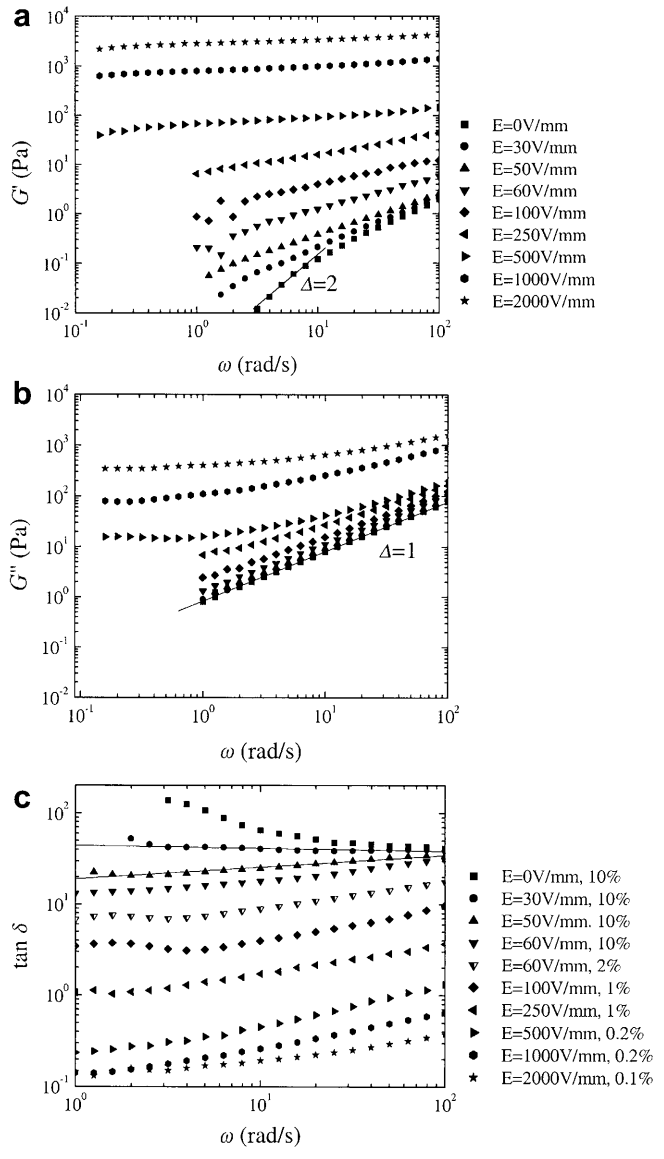

Fig. 5a–c Frequency dependence of linear viscoelastic properties for ERS107 (silica suspension with $\phi = 0.107$): **a** storage moduli G'; **b** loss moduli G''; **c** tan δ. The strain amplitudes vary with field strength, 10% for $E \leq 60$ V/mm, 1% for E = 100 and 250 V/mm, 0.2% for $E = 500$ and 1000 V/mm, and 0.1% for $E = 2000$ V/mm

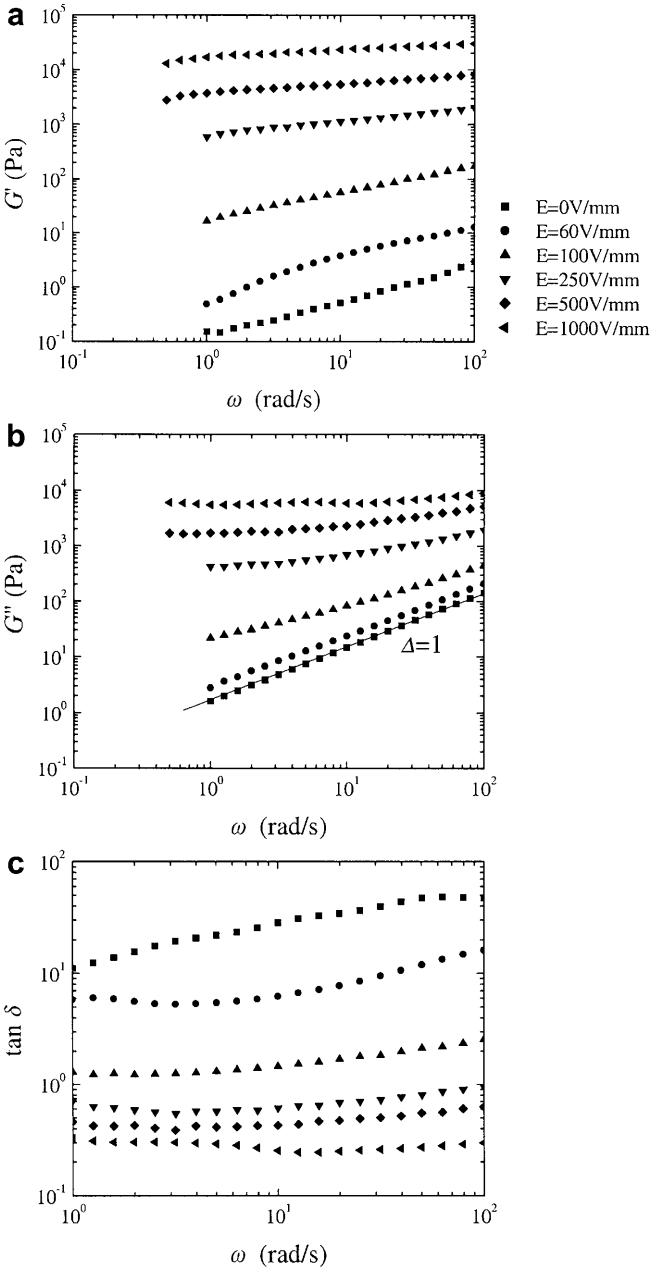

Fig. 6a–c Frequency dependence of linear viscoelastic properties for ERS171 (silica suspension with $\phi = 0.171$): **a** storage moduli (G'); **b** loss moduli (G''); **c** tan δ. The strain amplitudes at each field strength are 10% for $E \leq 60$ V/mm, 0.2% for $E = 100$ V/mm, 0.1% for $E = 250$, 500 V/mm, and 0.05% for $E = 1000$ V/mm

Steady shear viscosity – plastic flow and yield stress

ERS107 and ERS171 were probed in steady shear flow at shear rates from 0.1 to 100 s^{-1} and electric field strengths between 0 and 2000 V/mm (Fig. 7). In the absence of an electric field, both ERSs behaved like a Newtonian fluid (constant steady shear viscosity) in the entire range of shear rate. At low field strength $E = 250$ V/mm, ERS107 began to develop a yield stress, resulting in a low shear rate plateau in a logarithmic plot (Fig. 7a). The height of such plateau increased with field strength. In steady shear flow at intermediate rates, electric forces between particles were balanced with the fluid-dynamic forces. At low field strength the internal structure could not be maintained due to the dominating fluid dynamic forces. At high field strength ($E \geq 1000$ V/mm), the effect of the electric field was strong enough to dominate even the high shear rate behavior. ERS171 showed more pronounced shear effects than ERS107; a finite yield stress was observed at $E = 100$ V/mm and the

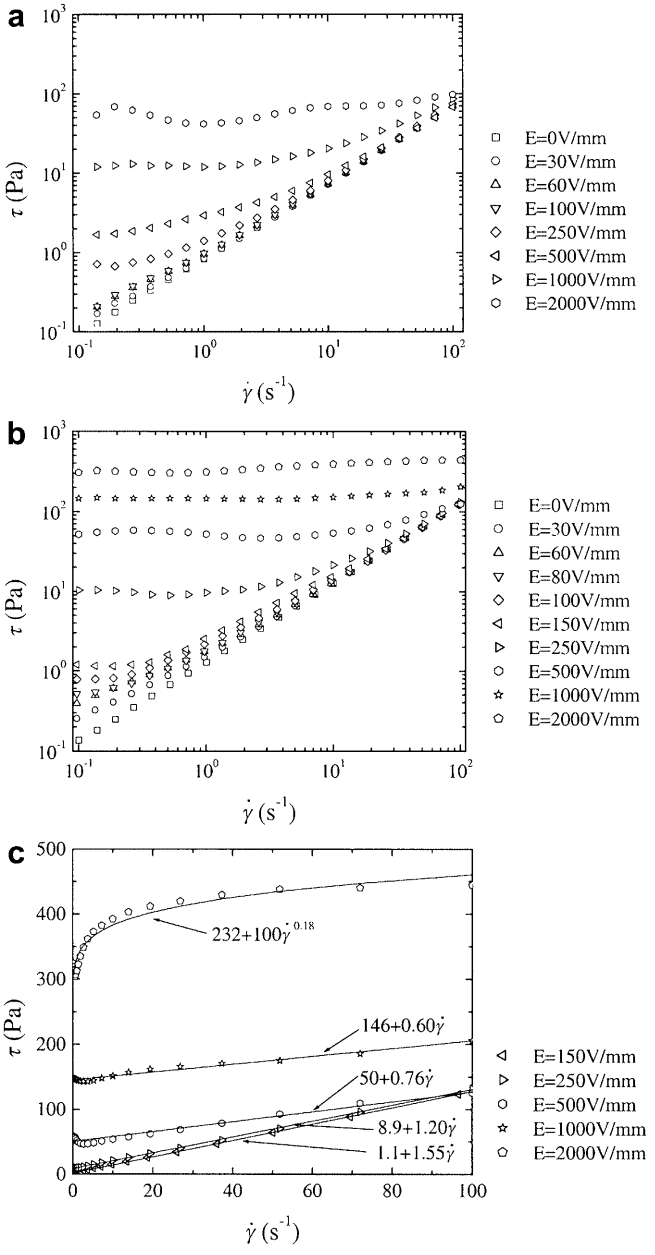

Fig. 7a–c Steady flow at increasing electric field strengths: **a** logarithmic plot of shear stress vs shear rate for ERS107; **b** logarithmic plot for ERS171; **c** linear plot for ERS171. For $100 \le E \le 1000$ V/mm, the Bingham model was sufficient. For $E = 2000$ V/mm, the Herschel-Bulkley model ($m = 100$ Pa.s^n, $n = 0.18$) was chosen because of significant shear-thinning

field effect at high shear rate began to manifest itself at $E \ge 500$ V/mm.

For moderate electric field strength (100∼1000 V/mm), stress extrapolation with a Bingham model gives an estimated yield stress value. Figure 7c (linear scale plot of Fig. 7b) illustrates the ability of the Bingham model to describe ERS171 in steady shear. However, the shear stress∼shear rate curve at $E = 2000$ V/mm cannot

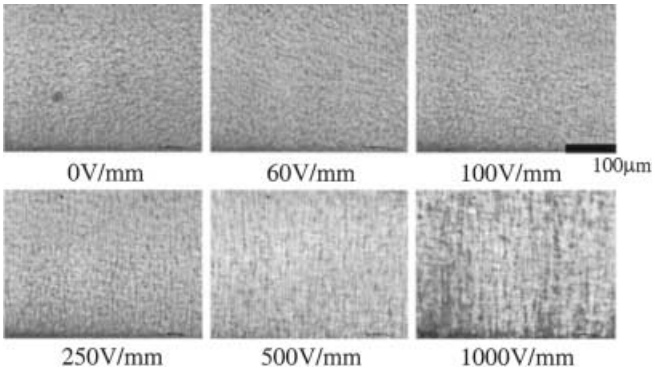

Fig. 8 Microstructures of silica suspension (ERS107) at the increasing electric field strength without shear flow (magnification: × 12.6)

be expressed by the linear Bingham model due to the pronounced shear-thinning (decreasing plastic viscosity). Therefore, the fitted yield stress of 232 Pa at this condition is obtained by the Herschel-Bulkley model, Eq. (4), which combines a yield stress with a power-law viscous component ($m = 100$ Pa.s^n and $n = 0.18$).

Optical microscopy observation

The optical microscope allowed direct observation of the microstructural patterns (ERS107) in the electric field at stationary conditions (Fig. 8). Even though the magnification of the microscope was too low to distinguish isolated particles as such, ordering phenomena could be observed. The suspension was not severely aggregated at 0 V/mm. Also, at low field strength of 60 V/mm, there was no noticeable movement of particles along the field lines. Strings of spheres started to develop at about 250 V/mm due to the long-range interacting electrostatic polarization forces. The density of strings increased with the applied field strength until, at $E \ge 500$ V/mm, the particle strings coalesced to columns, and the thickness of each column increased further with the field strength. The onset of formation for distinct columns ($E = 250$ V/mm) was found to coincide with the appearance of a finite yield stress, as seen in the case of ERS107 at Fig. 7a.

Discussion

The field-induced structuring of ERSs can be tuned to show the transition from viscoelastic liquid to viscoelastic solid. The transition occurs gradually and is clearly induced by the formation of particle aggregates, particle strings, and then columns. The sample-spanning particle structure is very fragile. A slight deformation can already induce unstable states. As a result, the dynamic moduli are strongly sensitive to the amplitude of strain,

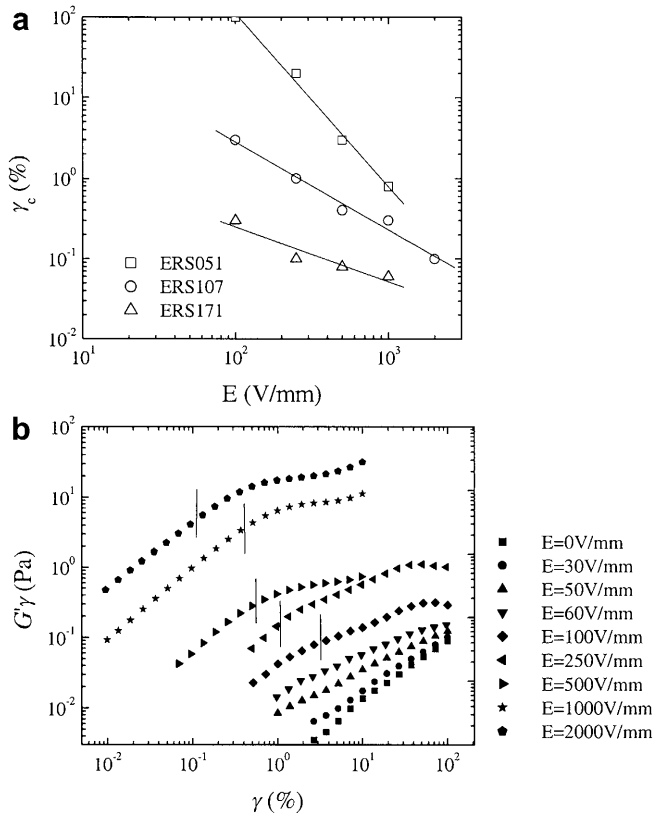

Fig. 9a, b Upper limiting strain and stress for linear viscoelasticity: **a** the limiting strain amplitude was measured at $\omega = 10$ rad/s; **b** in-phase stress component ($G'\gamma$), replotted with the data of Fig 3a. The vertical lines indicate the limit of linear viscoelasticity at each field strength

as seen in Fig. 3a,b. The limiting strain (γ_c) decreased linearity with electric field, Fig. 9a, and the corresponding stress (in-phase, $\tau' = G'\gamma$) goes up, Fig. 9b. The ERS becomes stiffer showing larger modulus, but starts to break at a smaller strain. Clearly, the in-phase stress linearly increases with strain within the linear viscoelastic limit (displayed as vertical lines in Fig. 9b), reaching an equilibrium or maximum which is reported as measure of the yielding or structural breakdown (Yang et al. 1986; Pan and McKinley 1997).

We have defined the limiting strain (γ_c) as the amplitude at which G' or G'' started to decrease. In strong electric fields ($E \geq 500$ V/mm), G' was a function of strain even at amplitudes lower than $\gamma = 0.1$–0.5%. However, at very low field strength (30∼60 V/mm), G'' was much larger than G' (see Fig. 3a), and the linear region for G' was not as clearly distinguishable any more. Here, we used the linearity limit of G'' for defining the value of γ_c. The limiting strain for linearity obtained for our ERS samples was at about the same level as reported in the literature (Jordan et al. 1991; Pan and McKinley 1997). Based on their point-dipole simulation studies, Parthasarathy and Klingenberg (1996) attributed the onset of nonlinearity to micro-rearrangement of particle strings.

Small amplitude oscillatory shear experiments are the preferred method to study rheological phenomena of the preserved structure; the small strain can directly probe these interactions while minimizing the influence of external flow fields. The string model in ERS composed of single particle thickness produced frequency-independent storage and loss moduli, as seen in simulated results of McLeish et al. (1991) and Klingenberg (1993). However, thick columns and their attached side branches do not behave as ideal strings due to the existence of short-range interactions in-between the columnar strings (Halsey 1992). Also, Pan and McKinley (1997) proposed the role of secondary structure between primary particle strings, which makes the structure of ERS more sensitive to the applied strain. Another complexity arises from the competition between electrostatic and fluid-dynamic forces (which can also be produced by the imposition of an electric field) acting on the particulate strings. It results in a crossover of dynamic structure and rheological response between the small and large frequency limit.

The $G'(\omega)$ and $G''(\omega)$ data at increasing electric field strengths could be compared with the evolving moduli of crosslinking polymers (Winter and Chambon 1986; Winter and Mours 1997; Mours and Winter 1998). Power-law dependence of G' and G'' is expected at frequencies that characterize the relaxation of internal modes on length scales where the system has a self-similar structure. In cases of non-uniform structural fluctuations, some systems showed no power-law relaxation (Richtering et al. 1992), or limited range as over 1.5 decades of frequency (Power et al. 1998). Deviation in the result of Power et al. (1998) was attributed to the non-ideal nature of the network, suggesting that the gelation model of Winter and Chambon (1986) can be applied for a measure of progressively increasing structural degree of system. The power law region of the present ERS was restricted to only about 2 decades (from 10^0 to 10^2 rad/s). At the lower frequencies below 10^0 rad/s, the samples simply could not transmit enough torque to be detected by our instrument (due to the small-strain conditions), especially in the range of low electric field ($E < 500$ V/mm).

Figures 4c and 5c illustrate the transition through a state with flat tan δ as expected for classical gelation, though it is a non-ideal system with only unidirectional connectivity. Such a directional gelation (DG) of a field-induced anisotropic structure was found to occur at the very low electric field strength. Figure 4c shows the transition of ERS051 silica suspension at an electric field of 60 V/mm (tan δ is independent of frequency), changing the slope from negative for a liquid to positive for a solid with further increase of electric field strength. For the ERS107, the critical field strength was even lower

($E = 30$ V/mm, see Fig. 5c). In the vicinity of this transition, the storage modulus is somewhat sensitive to the amplitude of strain, as seen in Fig. 3a. The magnitude of tan δ at 60 V/mm was still decreasing with decreasing amplitude (Fig. 10b), denoting less-fragile structure at lower strain. However, this sensitivity did not affect to change the slope in tan δ (see Fig 5c, for 60 V/mm cases), indicating that it was clearly a field-induced transition.

Unlike the ERS051 and ERS107, ERS171, the most concentrated suspension, did not exhibit such gelation transition. The slope of tan δ was already positive without electric field (Fig. 6c). The possible formation of water-bridges between the more closely packed particles (See et al. 1993) already caused sufficient connectivity for the ERS to show the solid behavior at low-amplitude dynamic shear. Martin et al. (1994) covered the surface of silica with organophilic silane coupling agent in order to remove the surface water. This effectively resulted in a model ERS for ideal (single particle thickness) and completely reversible string formation (probed by microscopy). However, probably due to the reduced adhesion on the electrodes as well as reduced particle polarizability, their ERS sample showed neither a finite yield stress nor a linear viscoelastic range, which make the dynamic viscoelastic study difficult. Therefore, sufficient connectivity and stable sample-spanning structures (especially binding on the electrodes) are important for a dynamic rheological study of field-induced gelation; a hydrated particle suspension is an appropriate system at low volume fraction where the interaction by water-bridge formation is negligible.

It should also be noted that at such low critical field strengths (30–60 V/mm), G'' was still substantially higher than G', although the power law dependence of G' and G'' was nearly identical both for ERS051 and ERS107 silica suspensions. Also the gel point is reached before sample-spinning, strings become visible in the microscopic image (see Fig. 8). A clear image of particle strings appeared at about 250 V/mm for ERS107. Here, the magnitude of G' and G'' was nearly similar at low frequencies, while G' became smaller than G'' with increasing ω.

Generally, the liquid-to-solid transition became evident in the following experimental observations (Winter and Mours 1997):

1. The diverging zero-shear viscosity (η_0) and dynamic viscosity at low frequency (η^*)
2. The limiting storage modulus (G') at low frequency

When the field-induced structure is fully developed in a well designed ERS, it generates a finite yield stress as well as diverging zero-shear viscosity. According to Barnes (1999), the existence of the yield stress for structured liquid could be shown when there is usually a small range of stress over which the viscosity changes dramatically (apparent yield stress). Indeed, an ERS can support a stress with no flow. This minimum upper (static) yield stress is defined as the minimum shear stress which is required to start a macroscopic flow in an initially static sample. This is also directly measurable by, for example, the vane geometry method (Nguyen and Boger 1985) although uniform electric field cannot be easily made for this fixture. On the other hand, using the appropriate model, the yield stresses could be extrapolated in the shear rate-stress data (Fig. 7). Here the extrapolated values, for example with the Bingham equation, correspond to the dynamic yield stresses (Kraynik 1990). Since the fragile particulate strings of ERS experience the rapid reconfiguration of the microstructure under constant shear, the upper yield stress and the dynamic yield stress value obtained by the yield stress equation are closely related but not exactly equivalent (Bonnecaze and Brady 1992).

The zero-shear viscosity grows with field strength and, at some characteristic value of E, a yield stress appears and grows at higher field strengths; see Fig. 10a. The data of ERS051 are not shown because the stress

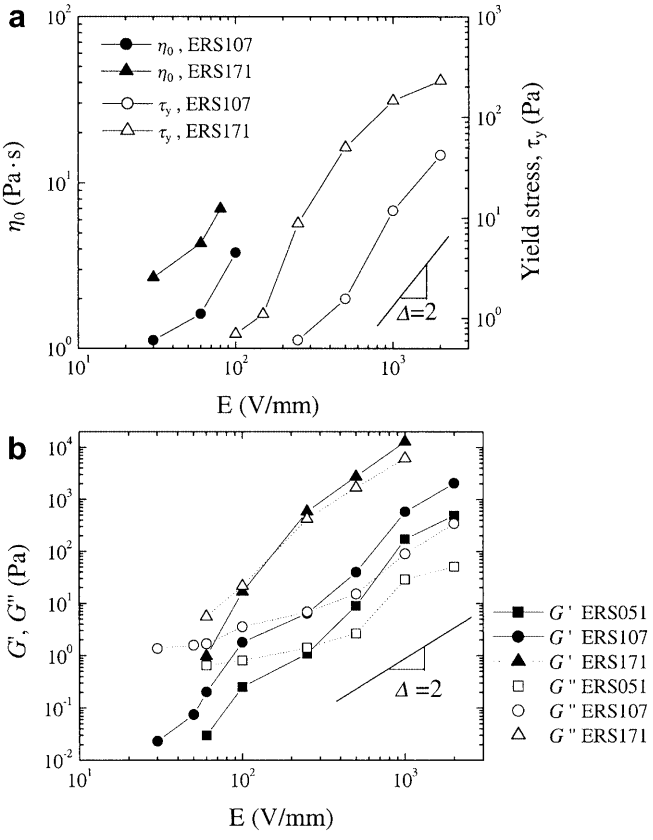

Fig. 10 **a** Diverging zero-shear viscosity and the development of yield stress, for the ERS107 and ERS171. **b** The storage and loss moduli at low frequency(ω), which are obtained at $\omega = 1$ rad/s for $E \leq 250$ V/mm and $\omega = 0.1$ rad/s for $E \geq 500$ V/mm

levels are too low (and, hence, uncertain) at low shear rates. Since the dynamic yield stress is related to the electrostatic energy, several experimental and theoretical studies support the E^2-dependence of yield stress (Bonnecaze and Brady 1992; Ostubo 1992). At high field, deviation from E^2-dependence (E^{Δ}, where $1 < \Delta < 2$) occurs as a result of charging effect in the solvent around the particles, or conduction between the adjacent semiconducting particles (Tang et al. 1995; Chin et al. 1998). Upon increasing the field strength from zero, the zero-shear viscosity η_0 increases due to the facilitated particle-particle interaction. Such field-dependent shear viscosities without yield stress were well characterized by Martin et al. (1994, 1998), reporting that an inverse power-law dependent shear viscosity could be explained by their independent droplet model; roughly prolate spheroidal aggregates tilt until electrical and fluid-dynamic torques balance. Figure 10a shows the liquid-to-solid transition of ERS at the vicinity of the appearance of yield stress. However, such diverging viscosity and equilibrium yield stress should be obtained by the extrapolation, and are not easy to determine for many cases.

In the absence of equilibrium modulus data, the storage and loss moduli (G', G'') at the lowest accessible frequency are useful for characterizing the low-field transition regime of ERSs; see Fig. 10b. Values of G', G'' were obtained at $\omega = 1$ rad/s for $E \leq 250$ V/mm and at $\omega = 0.1$ rad/s for $E \geq 500$ V/mm. G'' exceeds G' at zero field (not presented in such a logarithmic plot) and at very low field strength. The order inverts at an increased field strength value. The inversion happens at lower field strength as the volume fraction of ERS increases. This does, however, not indicate the gel point. As the field strength increased sufficiently, G'' grew proportionally with E^2 while G' grew with E at an even higher exponent. This indicates the existence of another short-range interaction contributing to the elasticity; coalescing of neighboring strings might enhance the column strength (Halsey 1992), or phase-separated water-bridges might form between the particles (See et al. 1993).

The schematic of Fig. 11 proposes a possible mechanism for the liquid-to-solid transition of ERS. Without a field, ERS is a suspension with random dispersion of particles without noticeable connectivity. At low field strength, local ordering of particles seems to take place in the bulk as well as near the wall (also by electrophoresis). The resultant particle aggregates resist shear flow when getting tilted due to local vorticity (Halsey et al. 1992; Martin et al. 1994). This will increase the dynamic viscosity (however, not plotted in this figure) as well as the low-frequency modulus (replacing the equilibrium modulus). The tan δ method provides an effective criterion for detecting the gel point of samples with such fragile connectivity.

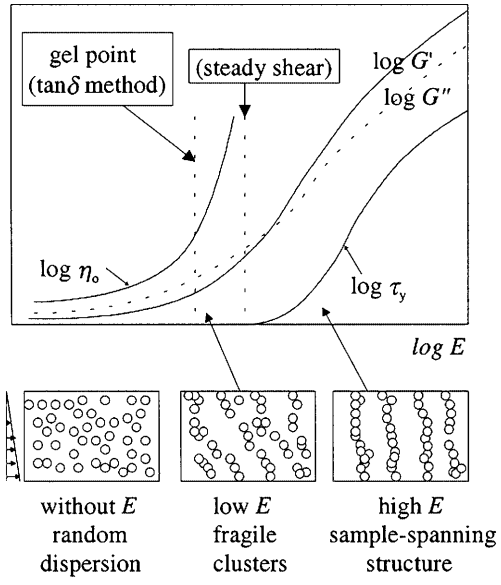

Fig. 11 Schematic of structure evolution during the field-induced liquid-to-solid transition for an ERS. The gel point of a static sample occurs at low field strength. Under steady shear, the transition gets shifted to higher field strength

The transition is more difficult to detect in a flow experiment, which suggests a yield stress at much higher field strength. Additional phenomena, such as diverging shear viscosity and yield stress, are also described in Fig. 11. The fragility of ordered ERS structures as well as continuous re-configuration in the vicinity of gel point results in a difference in their mechanical properties between small-amplitude dynamic shear and continuous shear flow. If wall-slip at the very low shear rate can be effectively eliminated, the yield stress might be realized even at lower field strength. It is also possible that the gel point by the tan δ method lies at a higher field if the effect of short-range force by the formation of water-bridge between particles can be avoided.

Conclusions

Field-induced particle assembly in an electro-rheological suspension (ERS) results in a liquid to solid transition which was observed under static (linear viscoelastic range) and under shear flow conditions. The linear, dynamic moduli adopt a low frequency power law behavior at very low field strength already. We attribute this intermediate power-law state to the gel point because the relaxation patterns are the same as in chemical gelation of crosslinking polymers. At the critical field strength of the gel point, distinct particle strings are not yet visible in the microscope. The sample spanning connectivity seems to be caused by

particle aggregates, both near the wall and in the bulk of the suspension. When the field strength is further increased, particle strings and then thicker columns develop across the sample. The field-induced transition of ERS, however, is complicated by anisotropic connectivity (directional effect), fragility (easily broken internally at small stress or strain), and development of a yield stress.

Steady shear behavior of ERS has the typical features of the Bingham or Herschel-Bulkley model, depending on particle concentration. A finite yield stress began to appear at a field strength which was higher than the (static) gel point. The yield stress appeared at a field strength at which the formation of particle strings had been observed in the microscope. Flow-induced breaking of connectivity and continued reformation of ordered structure gives rise to the yield stress under flow.

Acknowledgments This work was partially supported by the postdoctoral fellowship program of the Korea Science and Engineering Foundation (KOSEF). Additional financial support from National Environmental Technology Institute (NETI) at University of Massachusetts is appreciated. We also thank Prof. S.L. Hsu (University of Massachusetts) for letting us use his high voltage power generator throughout our study.

References

Barnes HA (1999) The yield stress – a review or '$\pi\alpha\nu\tau\alpha\ \rho\epsilon\iota$' – everything flows? J NonNewtonian Fluid Mech 81:133

Block H, Kelly JP (1988) Electro-rheology. J Phys D Appl Phys 21:1661

Bonnecaze RT, Brady JF (1992) Yield stress in electrorheological fluids. J Rheol 36:73

Chambon F, Winter HH (1987) Linear viscoelasticity at the gel point of a crosslinking PDMS with imbalanced stoichiometry. J Rheol 31:683

Chin BD, Lee YS, Park OO (1998) Effects of conductivity and dielectric behaviors on the electrorheological properties of poly(*p*-phenylene) suspensions. J Colloid Interface Sci 201:172

Davis LC (1992) Polarization forces and conductivity effects in electrorheological fluids. J Appl Phys 72:1334

Deinega YF, Vinogradov GV (1984) Electric fields in the rheology of disperse systems. Rheol Acta 23:636

Gamota DR, Filisko FE (1991) High frequency dynamic mechanical study of an aluminosilicate electrorheological material. J Rheol 35:1411

Goodwin JW, Markham GM, Vincent B (1997) Studies on model electrorheological fluids. J Phys Chem B 101:1961

Halsey TC (1992) Electrorheological fluids. Science 258:761

Halsey TC, Martin JE, Adolf D (1992) Rheology of electrorheological fluids. Phys Rev Lett 68:1519

Jordan TC, Shaw MT, McLeish TCB (1991) Viscoelastic response of electrorheological fluids. II. Field strength and strain dependence. J Rheol 35:441

Klingenberg DJ (1993) Simulation of the dynamic oscillatory response of electro-rheological suspensions: demonstration of a relaxation mechanism. J Rheol 37:199

Klingenberg DJ, Zukoski CF (1990) Studies on the steady-state behavior of electrorheological suspensions. Langmuir 6:15

Kraynik AH (1990) Comments on ER fluid rheology. Proceedings of 2nd International Conference on ER Fluids, p 445

Lee DY, Wereley NM (2000) Analysis of electro- and magneto-rheological flow mode dampers using Herschel-Bulkley model. In: Hyde TT (ed) Damping and isolation. Proceedings of SPIE Conference on Smart Materials and Structures, vol 3989

Marshall L, Zukoski CF, Goodwin JW (1989) Electric field effect on the rheology of non-aqueous concentrated suspensions. J Chem Soc Faraday Trans I 85:2785

Martin JE, Adolf D, Halsey TC (1994) Electrorheology of a model colloidal fluid. J Colloid Interface Sci 167:437

Martin JE, Odinek J, Halsey TC, Kamien R (1998) Structure and dynamics of electrorheological fluids. Phys Rev E 57:756

McLeish TCB, Jordan T, Shaw MT (1991) Viscoelastic response of electrorheological fluids. I. Frequency dependence. J Rheol 35:427

Mours M, Winter HH (1998) Relaxation pattern of endlinking polydimethylsiloxane near the gel point. Polym Bull 40:267

Nguyen QD, Boger DV (1985) Direct yield stress measurement with the vane method. J Rheol 29:335

Ostubo Y (1992) Electrorheological properties of silica suspension. J Rheol 36:479

Pan XD, McKinley GH (1997) Structural limitation to the material strength of electrorheological fluids. Appl Phys Lett 71:333

Parthasarathy M, Klingenberg DJ (1996) Electrorheology: mechanisms and models. Mater Sci Eng R17:57

Power DJ, Rodd AB, Peterson L, Boger DV (1998) Gel transition studies on nonideal polymer networks using small amplitude oscillatory rheometry. J Rheol 42:1021

Randall CA, McCauley DE, Bowen CP, Shrout TR, Messing GL (1994) High dielectric constant particulate materials for electrorheological fluids. In: Tao R, Roy GD (eds) Proceedings of 4th International Conference on Electrorheological Fluids. World Scientific, Singapore

Richtering HW, Gagnon KD, Lenz RW, Fuller RC, Winter HH (1992) Physical gelation of a bacterial thermoplastic elastomer. Macromolecules 25:2429

See H, Tamura H, Doi M (1993) The role of water capillary forces in electrorheological fluids. J Phys D Appl Phys 26:746

Tang X, Wu C, Conrad H (1995) On the conductivity model for the electrorheological effect. J Rheol 39:1059

Tlusty T, Safran SA (2000) Defect-induced phase separation in dipolar fluids. Science 290:1328

Tse KL, Shine AD (2000) Steady-state electrorheology of nematic poly(*n*-hexyl isocyanate) solutions. Macromolecules 33:3134

Wang X, Gordaninejad F (2000) Study of controllable fluid dampers in flow mode using Herschel-Bulkley model. In: Hyde TT (ed) Damping and isolation. Proceedings of SPIE Conference on Smart Materials and Structures, vol 3989

Winslow WM (1949) Induced fibrillation of suspensions. J Appl Phys 20:1137

Winter HH, Chambon F (1986) Analysis of linear viscoelasticity of a crosslinking polymer at the gel point. J Rheol 30:367–382

Winter HH, Mours M (1997) Rheology of polymers near their liquid-solid transitions. Adv Polym Sci 134:165

Yang MC, Scriven LE, Macosko CM (1986) Some rheological measurements on magnetic iron oxide suspensions in silicone oil. J Rheol 30:1015

Zukoski CF (1993) Material properties and the electrorheological response. Ann Rev Mater Sci 23:45